



Article

# Infill Designs for 3D-Printed Shape-Memory Objects

Daniel Koske and Andrea Ehrmann \*

Faculty of Engineering and Mathematics, Bielefeld University of Applied Sciences, 33619 Bielefeld, Germany; daniel.koske@fh-bielefeld.de

\* Correspondence: andrea.ehrmann@fh-bielefeld.de

**Abstract:** Shape-memory polymers (SMPs) can be deformed, cooled down, keeping their new shape for a long time, and recovered into their original shape after being heated above the glass or melting temperature again. Some SMPs, such as poly(lactic acid) (PLA), can be 3D printed, enabling a combination of 3D-printed shapes and 2D-printed, 3D-deformed ones. While deformation at high temperatures can be used, e.g., to fit orthoses to patients, SMPs used in protective equipment, bumpers, etc., are deformed at low temperatures, possibly causing irreversible breaks. Here, we compare different typical infill patterns, offered by common slicing software, with self-designed infill structures. Three-point bending tests were performed until maximum deflection as well as until the maximum force was reached, and then the samples were recovered in a warm water bath and tested again. The results show a severe influence of the infill pattern as well as the printing orientation on the amount of broken bonds and thus the mechanical properties after up to ten test/recovery cycles.

**Keywords:** poly(lactic acid) (PLA); shape-memory polymer (SMP); fused deposition modeling (FDM); 3D printing; infill pattern



**Citation:** Koske, D.; Ehrmann, A.

Infill Designs for 3D-Printed Shape-Memory Objects. *Technologies* **2021**, *9*, 29. <https://doi.org/10.3390/technologies9020029>

Academic Editor: Roberto Bernasconi

Received: 27 March 2021

Accepted: 13 April 2021

Published: 16 April 2021

**Publisher's Note:** MDPI stays neutral with regard to jurisdictional claims in published maps and institutional affiliations.



**Copyright:** © 2021 by the authors. Licensee MDPI, Basel, Switzerland. This article is an open access article distributed under the terms and conditions of the Creative Commons Attribution (CC BY) license (<https://creativecommons.org/licenses/by/4.0/>).

## 1. Introduction

Shape-memory polymers (SMPs) can recover their initial shape after deformations, triggered by an external stimulus, which is, in many cases, heat [1]. These properties are highly interesting for research and development and led to the development of many new polymers and polymer blends showing a shape-memory effect [2]. Typical applications can be found in spacecraft, biomedicine or smart textiles [3–5], with SMPs having different shapes such as bulk materials, films or foams [6–8].

Another possibility to create objects from SMPs is offered by 3D printing, e.g., stereolithography of fused deposition modeling (FDM) [9]. One of the materials most often used in 3D printing, poly(lactic acid) (PLA), shows such shape-memory properties [10]. It has, however, the disadvantage that it can only be elongated by ~10% until it breaks [11]. This leads to the question of how to avoid breaks by sophisticated constructions of samples.

Langford et al. used origami-inspired structures for this purpose and found that especially herringbone tessellated tubes could be strongly compressed and recovered afterwards, making them usable for biomedical scaffolds [12]. A simpler origami structure was suggested by Mehrpouva et al., who printed a flat structure foldable into a pyramid at higher temperatures [13].

More common structures were investigated by different groups, e.g., honeycomb, 3D honeycomb or gyroid structures, which are typical infill patterns, offered by many slicer programs [14–17]. Here, however, the general problem occurred that recovery after cold deformation was never perfect, with recovery ratios clearly below 100% due to undesired broken bonds.

Here, we perform three-point bending tests on test samples with different infill patterns, partly chosen from those offered by the slicer software, partly self-developed. Our results show that not only the infill pattern but also the printing orientation has a significant

impact on the recovery properties and lead to suggestions on how to improve recovery after cold deformation.

## 2. Materials and Methods

The samples used in this study were printed using a MEGA-S FDM 3D printer (ANYCUBIC; Shenzhen Anycubic Technology Co., Ltd., Shenzhen, China). With a nozzle diameter of 0.4 mm, a layer thickness of 0.2 mm was selected for the first layer and 0.12 mm for the other layers. The printing temperature was set at 200 °C and the heating bed temperature was set at 60 °C constant.

The test specimens made of PLA (GIANTARM PLA filament 1.75 mm, silver; no additives included to increase crystallinity [18]) were designed and printed with dimensions of 120 mm × 15 mm × 6 mm according to polymer test specimens (ISO 20753:2018). In order to investigate the influence of the filling pattern alone, no wall contours were printed, so the entire specimens were deflected only on the filling pattern and the lower and upper support plates of 1 mm each. The main dimensions were kept for the three-point bending test, and only the internal structure was changed.

The following support patterns and infill densities were applied to the specimens (Table 1): pattern line with 100% infill and 80% printing speed (LN100); pattern gyroid with 15% infill and 60% printing speed (GY15); pattern octet with 15% infill and 60% print speed (OC15); and self-designed filling structures in the form of hollow cylinders with 100% infill and 60% printing speed (ZHR100), a leaf spring construction (LP100) and a combination of the two (EW100). Some of the samples (ZHR100, LP100 and EW100) were printed lying flat on the printing bed as well as on the long edge. Table 1 shows all samples used here.

**Table 1.** Samples under examination in this study.

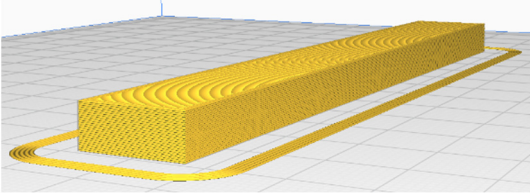
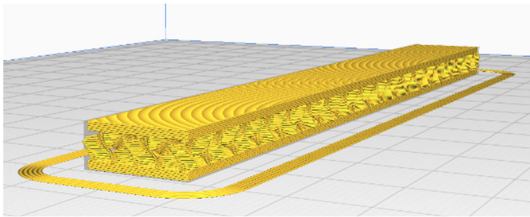
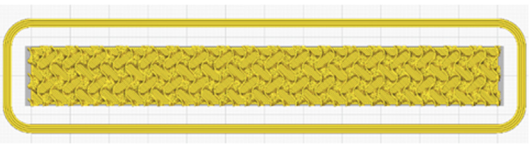
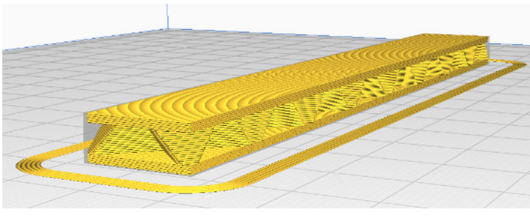
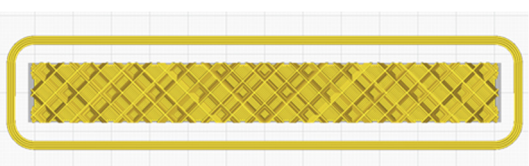
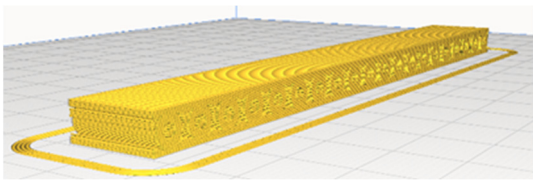
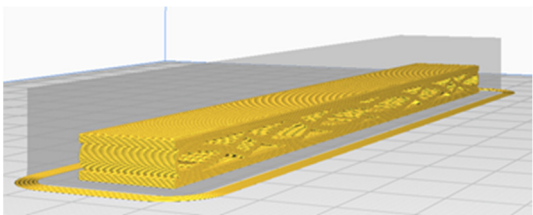
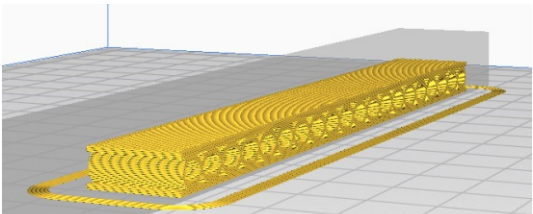
Sample Name	Main View	Top View/Front View
LN100		
GY15		
OC15		

Table 1. Cont.

Sample Name	Main View	Top View/Front View
ZHR100		
LP100		
EW100		

These samples were examined by a three-point bending test, using a universal testing machine (Kern & Sohn, Balingen-Frommern, Germany). Generally, a minimum of 4 specimens for each sample were examined, three of which were bent until breaking or until reaching the maximum deflection possible in the system. The fourth one was bent until the previously measured point of maximum force was reached and then relaxed and recovered in a water bath of  $(60 \pm 1)^\circ\text{C}$  for 1 min, before it was cooled down in another water bath at room temperature for 1 min. Since the aim of this investigation was avoiding broken areas, not optimization of the recovery process, these values were kept unchanged [19]. This temperature was chosen since amorphous PLA, as it typically is produced by 3D printing without a following heat treatment, has a glass transition temperature around  $56^\circ\text{C}$  [20,21] which was verified in previous tests [22]. It should be mentioned that using filaments from different producers, and even using a filament of different color from the same producer, may lead to different results as most producers do not mention possible additives. In particular, so-called high-temperature PLA (HT-PLA) includes different additives to increase crystallinity and, correspondingly, the glass transition temperature [18], enabling even autoclaving at  $121^\circ\text{C}$  without deformation of the sample [23].

For the optical examinations of the samples after the tests, a digital microscope, Camcolms2 (Velleman, Gavere, Belgium), was used.

### 3. Results and Discussion

Figure 1 depicts the three-point bending tests of the specimens shown in Table 1. For the self-designed infill patterns, samples were printed lying on the flat side as well as on the long edge.

As expected, the completely filled sample LN100 shows the highest maximum force. For the possible deflection of  $\sim 17.5$  mm, none of them broke.

The gyroid infill was found advantageous in another study working with cubes in which a linear object was pressed till half of the original height [15–17]. Here, it shows, by far, the lowest maximum force. The sudden drop in the force around 5–7 mm deflection,

visible in Figure 1b, is correlated with a delamination inside the infill, fully separating the top and bottom layers along one half of the respective specimen.

Sample OC15 shows a similar slope of the curve to LN100. Interestingly, the maximum force is approximately half the value found for LN100, while the infill was only chosen as 15%, showing that this infill performs better in relation to the sample mass than the completely filled sample.

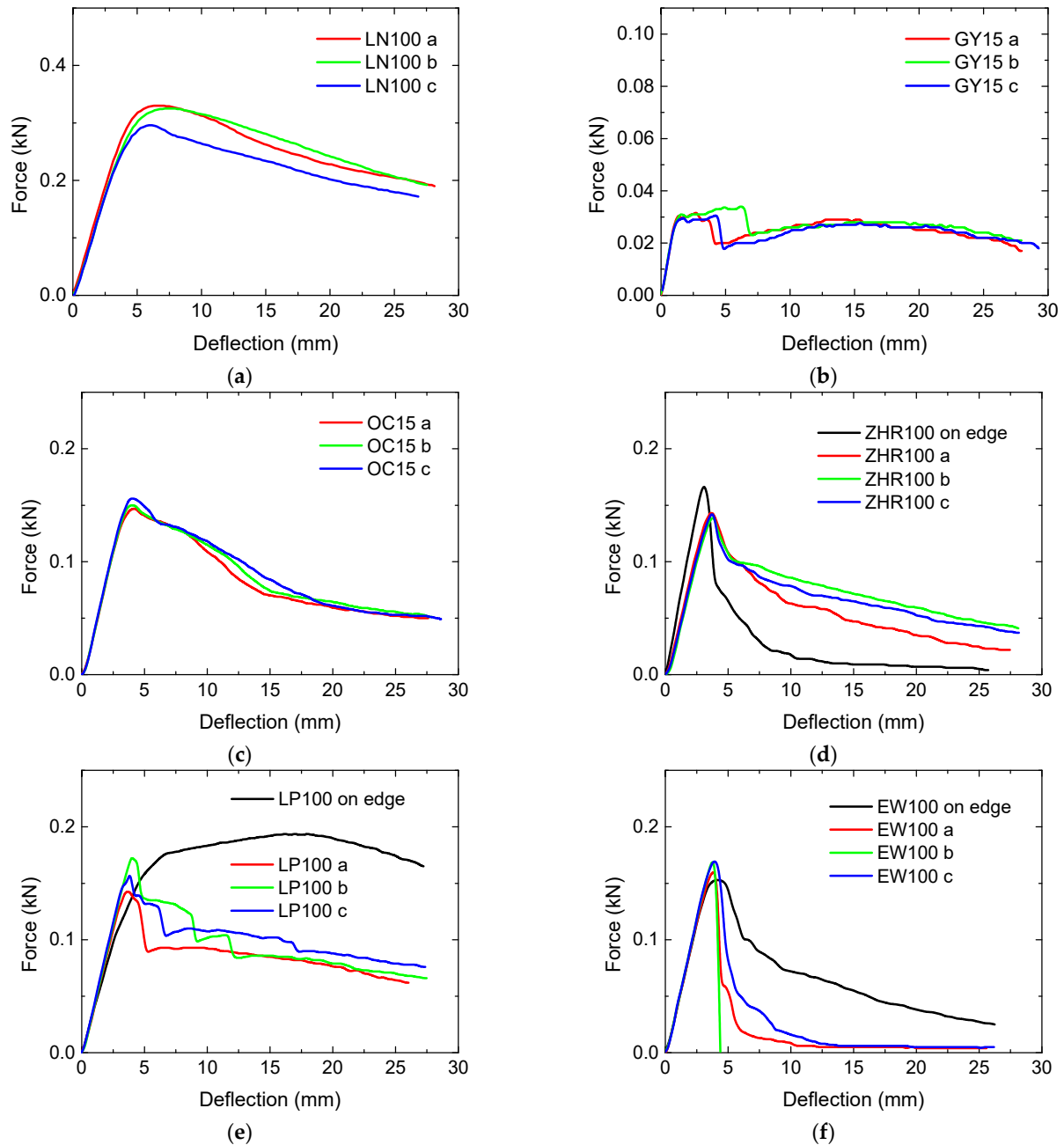


**Figure 1.** Three-point bending tests of samples with different infill patterns: (a) LN100; (b) GY15; (c) OC15; (d) ZHR100 including one specimen printed on the long edge; (e) LP100 including one specimen printed on the long edge; and (f) EW100 including one specimen printed on the long edge. Y-axis scales differ.

The samples with the first self-designed infill pattern, ZHR100, showed only a very narrow maximum, indicating that this infill will not work very well in repeated tests where deflection is planned to end at the point of maximum force. In all cases, the samples

showed a nearly completely broken lower plate at the position of the bending line. Similar effects are visible for samples LP100 and EW100.

Comparing the samples printed on the long edge, this has a slightly higher, but even narrower, peak for ZHR100, making this sample even less suitable for recovery tests than the original printing direction. For sample EW100, the opposite effect occurs. For sample LP100, however, a completely different shape is visible. Here, a very broad maximum is found, making this sample printed on the edge highly interesting for recovery tests. Due to the width of this curve, tests can be performed for a broad range of deflections.

The corresponding microscopic images of the samples after the bending tests (always specimen “a” in Figure 1) are shown in Figure 2.

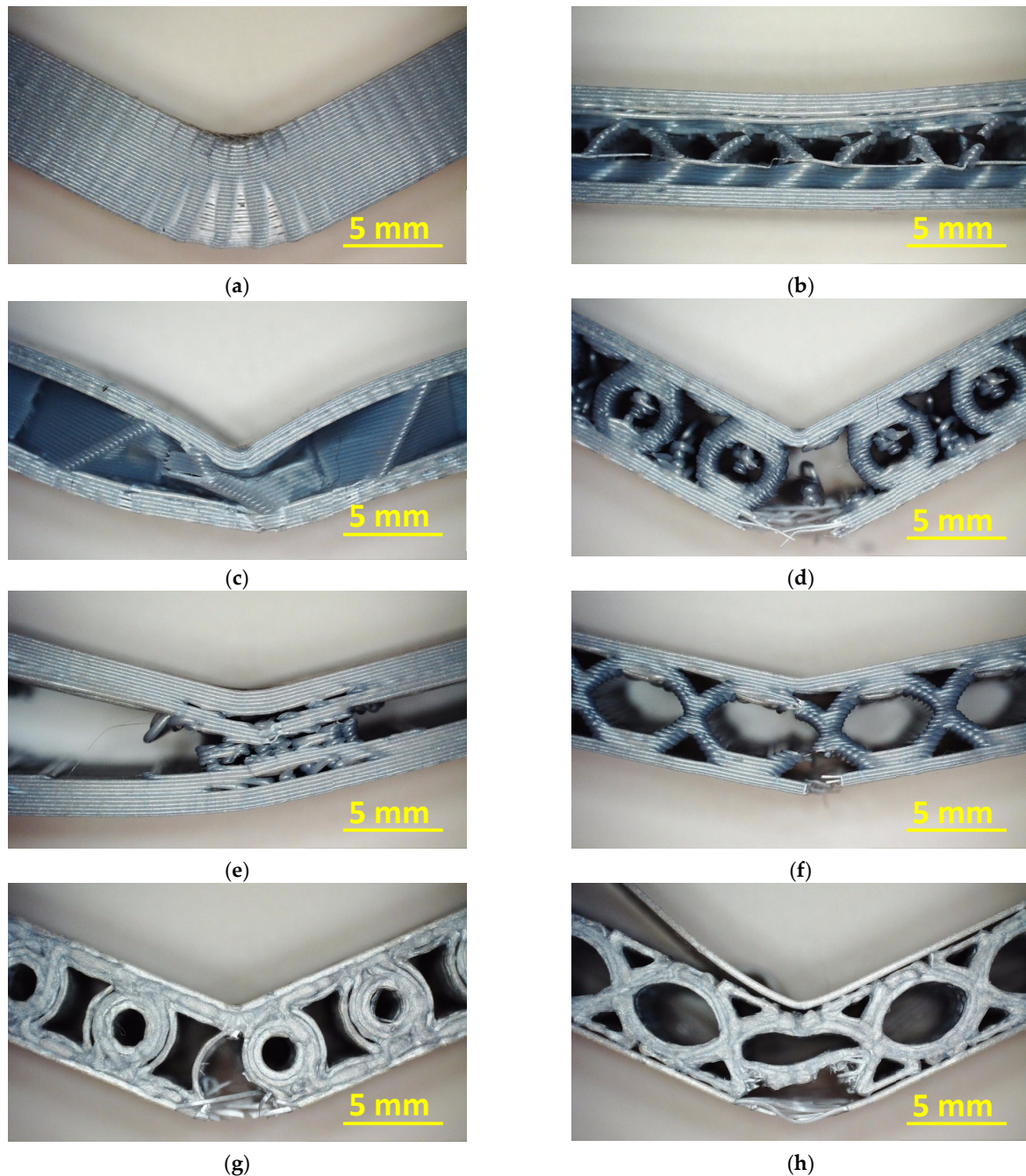


**Figure 2.** Microscopic images taken after three-point bending tests of samples with different infill patterns: (a) LN100; (b) GY15; (c) OC15; (d) ZHR100; (e) LP100; (f) EW100; (g) ZHR100 printed on the long edge; and (h) EW100 printed on the long edge. Sample LP100, printed on the long edge, will be shown later.

Sample LN100 (Figure 2a) shows a large area with stress whitening marks and, correspondingly, has a large residual strain after maximum deformation. GY15 (Figure 2b), oppositely, seems to have retained the original flat shape; however, in the right part of the sample, there are disrupted connections visible, being part of the full separation in the right half of the sample after the bending test. While samples OC15 (Figure 2c) and LP100 (Figure 2e) show residual deformations of the infill pattern, the other samples include broken strands along the lower plate of the sample where the pressure was applied.

Figure 3 shows the results of recovery tests during 10 cycles per sample, performed on the different specimens printed lying flat on the printing bed. Again, qualitative and quantitative differences between the infill patterns are visible.

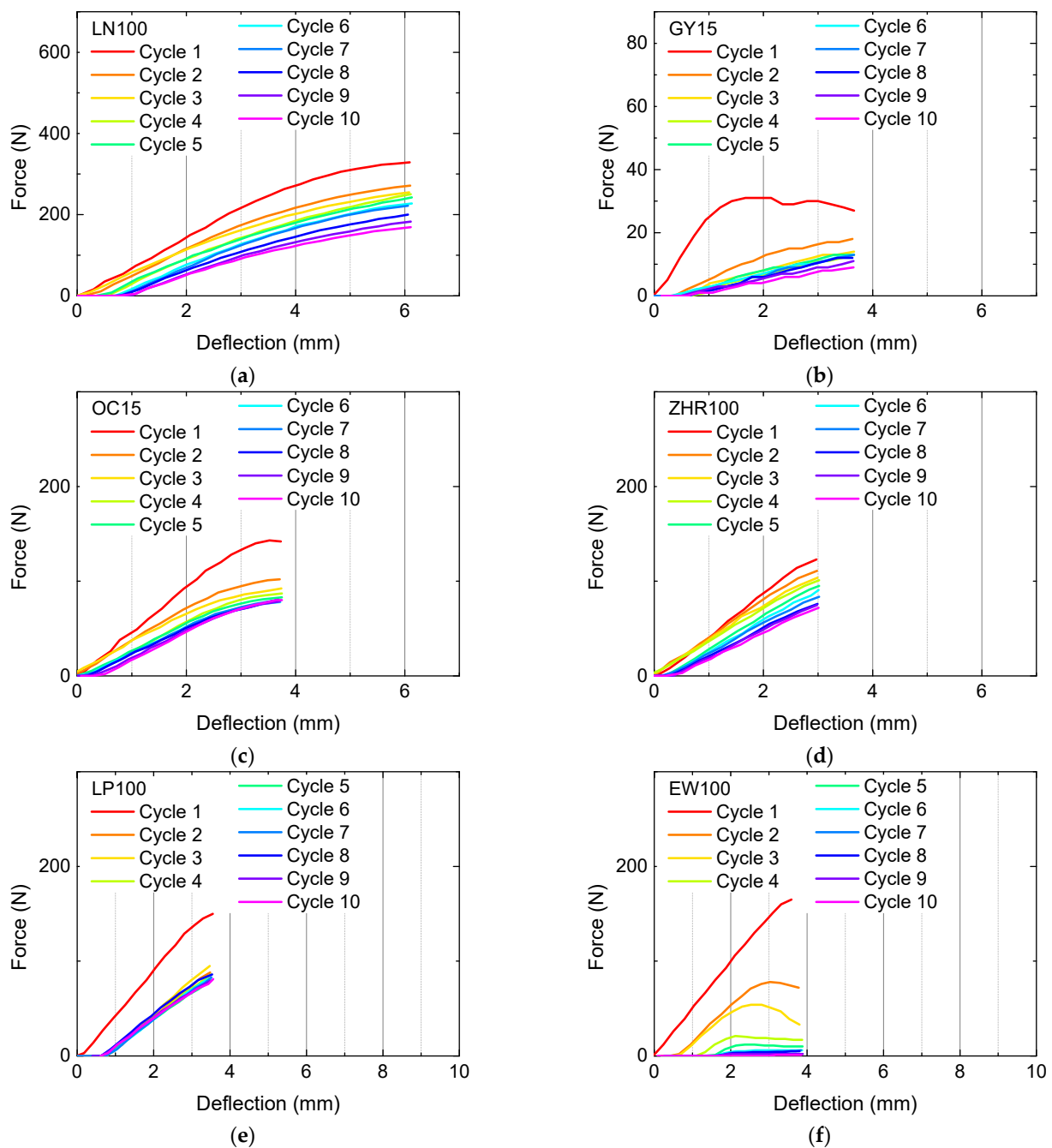


**Figure 3.** Bending and recovery tests of samples with different infill patterns: (a) LN100; (b) GY15; (c) OC15; (d) ZHR100; (e) LP100; and (f) EW100. Y-axis scales differ. Bending was performed till the deflection at which maximum force occurred, as measured in the previous tests.

For samples LN100 and ZHR100, the reduction in the maximum force after the first cycle is not much more pronounced than the consecutive reductions after the following cycles. Apparently, these infill patterns are better suited for bumpers, etc., which are normally damaged once or only a few times, as compared to the other samples showing a strong deviation between the first and the following cycles. The gyroid pattern shows a wave-like shape of the first force–deflection curve, similar to previous experiments with this pattern [15–17], and a relatively strong deviation between the first and second cycles, while the following cycles show relatively similar forces at identical deflections. However, none of the curves are smooth, which can be attributed to breaks of small connections occurring again and again.

The strongest deviations between the first and the second cycle are visible for sample LP100, while EW100 is nearly fully broken after 10 cycles, indicated by the very low forces measured at maximum deflection.

The corresponding microscopic images, taken after 10 bending and recovery cycles, are depicted in Figure 4. While all these samples show a slight residual strain, broken bonds are only visible in the lower part of EW100 (Figure 4f), indicating that the residual strain is correlated with changes in the material rather than with broken structures.

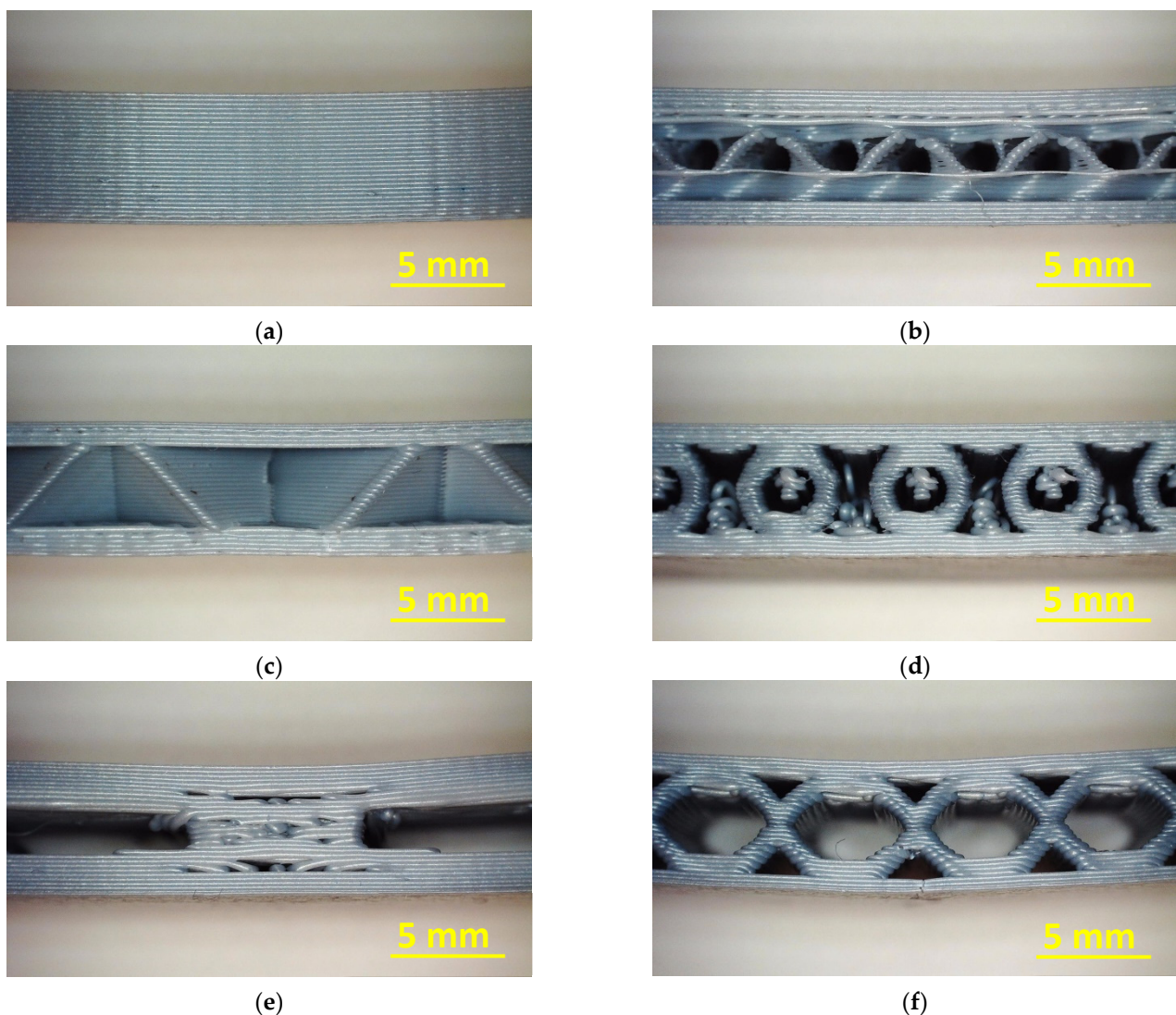


**Figure 4.** Microscopic images taken after 10 cycles of three-point bending and recovery tests of samples with different infill patterns: (a) LN100; (b) GY15; (c) OC15; (d) ZHR100; (e) LP100; and (f) EW100.

Next, Figure 5 shows the same tests, performed on sample LP100, printed on the edge. As mentioned before, due to the broad force maximum, different maximum deflections were chosen.

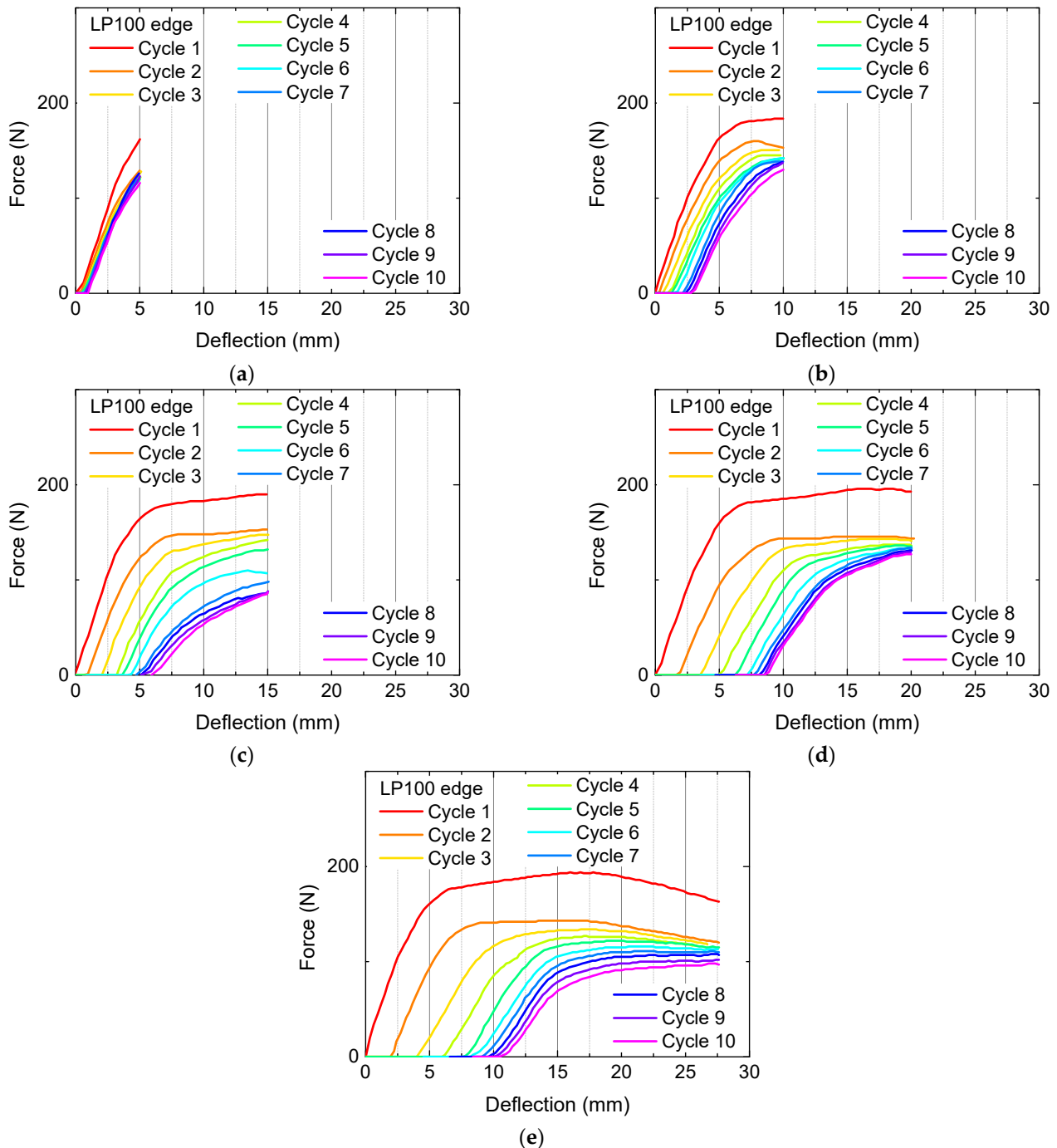


**Figure 5.** Bending and recovery tests of sample LP100, printed on the long edge, with different maximum deflections: (a) 5 mm; (b) 10 mm; (c) 15 mm; (d) 20 mm; and (e) 17.5 mm.

In all cases, the force differences between the first and the second curve are relatively large. In addition, the slopes of the curves differ not only for different cycles but also depending on the maximum deflection chosen. On the other hand, especially for the samples tested with a maximum deflection of 20 mm (Figure 5d), the forces reached at maximum deflection are quite similar for cycles 2–10, making this infill especially suitable for repeated deformations.

The corresponding microscopic images, taken after 10 bending and recovery tests each, are depicted in Figure 6. As expected, larger maximum deformations lead to larger residual strain. It should be mentioned that the full break visible in Figure 6c as well as the stress whitening observable in Figure 6d,e occurred usually after the first test cycle, after which no strong deviations were observed anymore, corresponding to Figure 5 showing that the largest force decrease occurs after the first cycle.

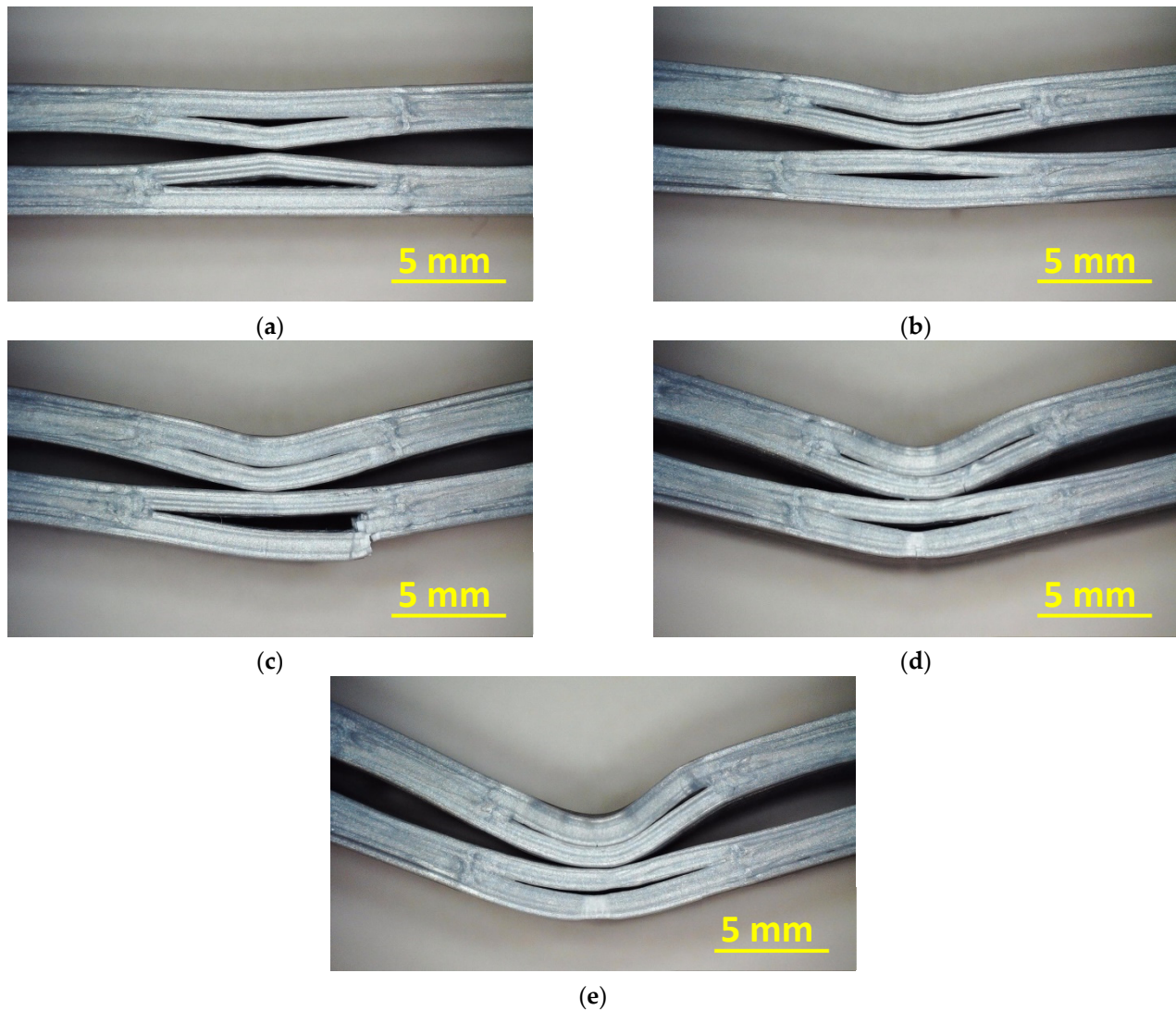


**Figure 6.** Microscopic images taken after 10 cycles of three-point bending and recovery tests of sample LP100, printed on the long edge, with different maximum deflections: (a) 5 mm; (b) 10 mm; (c) 15 mm; (d) 20 mm; and (e) 17.5 mm.

At the same time, these images suggest a possible optimization by varying the distance between the upper and lower halves of the leaf spring in the middle of the sample.

To compare the aforementioned residual strain quantitatively, Figure 7 depicts this value for all recovery tests shown here.

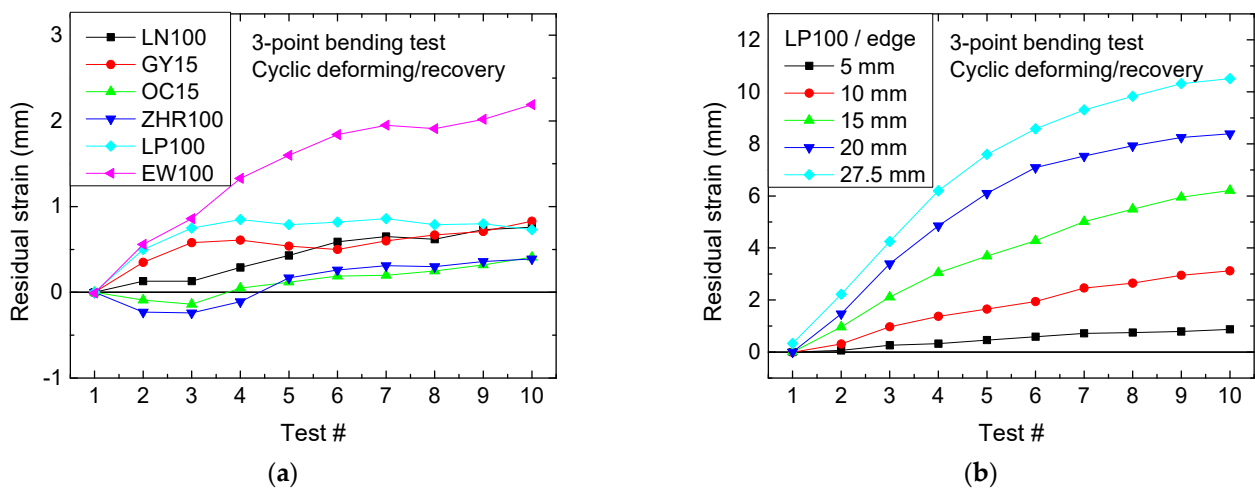


**Figure 7.** Residual strain of (a) samples printed flat; (b) sample LP100, printed on the edge, tested with different maximum deflections between 5 and 27.5 mm. Y-axis scales differ.

Amongst the samples printed flat on the printing bed (Figure 7a), EW100 shows the largest residual strain after 10 test cycles. For the infill patterns ZHR100 and OC15, the residual strain is firstly negative, meaning that the recovery process slightly overcompensates the deformation in the first three-point bending tests. This behavior was also found in previous tests, depending on the orientation of the impact [15–17].

For samples LP100, printed on the edge (Figure 4b), a clear correlation between the maximum deflection and residual strain is visible. Correspondingly, for the partly quite large deformation, residual strain values are reached which are much higher than those of the samples printed flat on the printing bed which were less bent.

Comparing these results with literature values is not easy since the test setups vary broadly. In many cases, researchers aim at the so-called 4D printing, meaning that deformation occurs above the glass transition temperature so that breaking of the samples is not to be expected [13,24–27]. Here, typically, recovery ratios near 100% are reached, if they are investigated at all; in many cases, one deformation is used to reach the desired final state.

In previous experiments of our group, cubes printed with different infill patterns and infill ratios were cold deformed along a linear impact area [15–17]. Here, the strong impact (with a depth of half the cube height) resulted generally in broken bonds which weakened the structure in subsequent test cycles. Similar to samples ZHR100 and OC15 (Figure 7a), a negative residual deformation was found in some cases, depending on the orientation of the applied pressure with respect to the printing orientation and thus to the infill pattern [17].

Senatov et al. compared pure PLA with PLA blended with hydroxyapatite (HA) to gain a certain self-healing effect by narrowing cracks after cold deformation. They found a shape recovery of 96–98% for the first cycle; however, delamination of the PLA sample already after the second cycle and of the PLA/HA sample after the third cycle, using porous structures, occurred [28]. Oppositely, here, most samples could be deformed without delamination or full break for the first ten test cycles. Nevertheless, it must be mentioned that the pressure was applied in a different way in Senatov’s study, making it again hard to compare with our results. In another study, Senatov et al. found decreasing recovery stress values with increasing numbers of warm deformation (above the glass transition temperature) and recovery cycles, with PLA samples breaking after three cycles in this case, while PLA/HA samples could be recovered after warm deformation for a minimum of 10 cycles [29].

In the literature, three-point bending tests of PLA at low temperatures followed by recovery above the glass transition temperature are scarce. Liu et al. programmed samples from PLA and SiC/C/PLA into bent shapes or stretched them at a temperature

of 90 °C and measured recovery at the same temperature, finding approximately 100% shape recovery [30]. Similarly, Dong et al. deformed three-point bending samples of PLA and PLA-grafted cellulose nanofibers above their glass transition temperature and found no difference between the recovery rates of these materials [31]. Liu et al. investigated a special textile-inspired structure in three-point bending tests; however, recovery tests were again performed after bending at higher temperatures [32].

As these examples show, research on the recovery of PLA after cold deformation is scarce and should be further extended to enable production of safety clothing, bumpers, etc., with shape recovery properties.

#### 4. Conclusions

Three-point bending test samples were 3D printed from the shape-memory polymer PLA. Different infill patterns were chosen, some of which are typically given by common slicing software, while others were self-designed. For the latter, samples were printed lying flat on the printing bed or placed on the long edge. Besides testing samples up to maximum deflection, the specimens were subjected to a deflection until the maximum force was reached, recovered in a warm water bath, tested again, etc.

While the completely filled sample showed a smooth slope of the force–deflection curves and similar force reductions after each recovery cycle, samples with a gyroid or octet infill showed a stronger force reduction from the first to the second cycle, making these patterns less suitable for situations in which only few damages are expected.

Amongst the self-designed infill patterns, the leaf spring construction printed on the long edge showed, by far, the most interesting behavior. The very broad range of the approximate maximum force makes it suitable for security objects, such as bumpers, and allows recovery after different deflections. Here, nevertheless, it must be taken into account that the residual strain is increased with increasing maximum deflection.

These experiments show the strong impact of such infill patterns and, in some cases, of the printing orientations, suggesting further research to create structures with a similar broad range of the approximate maximum force to that in the leaf spring pattern, but, in addition, with a smaller residual strain, in order to make such structures technologically better usable.

Another aspect which will be taken into account in a future study is the impact of additives or fillers, as they are partly available in the so-called HT-PLA [23], and of a heat post-treatment which may both increase crystallinity to a certain amount [22] and thus not only the glass transition temperature but also the mechanical properties at room temperature.

Since investigations of recovery after low-temperature deformation are scarcely found in the literature, many more experiments are necessary to optimize structures and materials for 3D-printed SMPs for the potential use in bumpers, safety clothing and other objects which are deformed accidentally and could be more sustainable if they were to be recoverable at nearly 100%.

**Author Contributions:** Conceptualization, D.K. and A.E.; methodology, D.K. and A.E.; formal analysis, A.E.; investigation, D.K. and A.E.; writing—original draft preparation, A.E. and D.K.; writing—review and editing, D.K. and A.E.; visualization, D.K. and A.E. Both authors have read and agreed to the published version of the manuscript.

**Funding:** This research received no funding.

**Institutional Review Board Statement:** Not applicable.

**Informed Consent Statement:** Not applicable.

**Data Availability Statement:** The data presented in this study are fully available in this article.

**Conflicts of Interest:** The authors declare no conflict of interest.

## References

1. Meng, H.; Hu, J.L. A brief review of stimuli-active polymers responsive to thermal, light, magnetic, electric, and water/solvent stimuli. *J. Intell. Mater. Syst. Struct.* **2010**, *21*, 859–885. [[CrossRef](#)]
2. Mather, P.T.; Luo, X.F.; Rousseau, I.A. Shape memory polymer research. *Annu. Rev. Mater. Res.* **2009**, *39*, 445–471. [[CrossRef](#)]
3. Blachowicz, T.; Pajak, K.; Recha, P.; Ehrmann, A. 3D printing for microsattellites—Material requirements and recent developments. *AIMS Mater. Sci.* **2020**, *7*, 926–938. [[CrossRef](#)]
4. Metcalfe, A.; Desfaits, A.-C.; Salazkin, I.; Yahiab, L.; Sokolowskic, W.M.; Raymonda, J. Cold hibernated elastic memory foams for endovascular interventions. *Biomaterials* **2003**, *24*, 491–497. [[CrossRef](#)]
5. Meng, Q.H.; Hu, J.L.; Yeung, L.Y. An electro-active shape memory fibre by incorporating multi-walled carbon nanotubes. *Smart Mater. Struct.* **2007**, *16*, 830–836. [[CrossRef](#)]
6. Lu, H.B.; Liu, Y.J.; Leng, J.S.; Du, S.Y. Qualitative separation of the physical swelling effect on the recovery behavior of shape memory polymer. *Europ. Polym. J.* **2010**, *46*, 1908–1914. [[CrossRef](#)]
7. Fu, C.-C.; Grimes, A.; Long, M.; Ferri, C.G.L.; Rich, B.D.; Thosh, S.; Ghosh, S.; Lee, L.P.; Gopinathan, A.; Khine, M. Tunable nanowrinkles on shape memory polymer sheets. *Adv. Mater.* **2009**, *21*, 4472–4476. [[CrossRef](#)]
8. Tobushi, H.; Hayashi, S.; Hoshio, K.; Miwa, N. Influence of strain-holding conditions on shape recovery and secondary-shape forming in polyurethane-shape memory polymer. *Smart Mater. Struct.* **2006**, *15*, 1033–1038. [[CrossRef](#)]
9. Chua, C.K.; Leong, K.F.; Lim, C.S. *Rapid Prototyping: Principles and Applications*, 2nd ed.; World Scientific Publishing Co. Pte. Ltd.: Singapore, 2003.
10. Wojtyła, S.; Klama, P.; Baran, T. Is 3D printing safe? Analysis of the thermal treatment of thermoplastics: ABS, PLA, PET, and nylon. *J. Occup. Environ. Hyg.* **2017**, *14*, D80–D85. [[CrossRef](#)]
11. Xu, J.; Song, J. Polylactic acid (PLA)-based shape-memory materials for biomedical applications. In *Shape Memory Polymers for Biomedical Applications*; Yahia, L.H., Ed.; Woodhead Publishing: Cambridge, UK, 2015; pp. 197–217.
12. Langford, T.; Mohammed, A.; Essa, K.; Elshaer, A.; Hassanin, H. 4D printing of origami structures for minimally invasive surgeries using functional scaffold. *Appl. Sci.* **2021**, *11*, 332. [[CrossRef](#)]
13. Mehrpouya, M.; Azizi, A.; Janbaz, S.; Gisario, A. Investigation on the functionality of thermoresponsive origami structures. *Adv. Eng. Mater.* **2020**, *22*, 2000296. [[CrossRef](#)]
14. Mehrpouya, M.; Gisario, A.; Azizi, A.; Barletta, M. Investigation on shape recovery of 3D printed honeycomb sandwich structure. *Polym. Adv. Technol.* **2020**, *31*, 3361–3365. [[CrossRef](#)]
15. Ehrmann, G.; Ehrmann, A. Shape-memory properties of 3D printed PLA structures. *Proceedings* **2021**, *69*, 6.
16. Ehrmann, G.; Ehrmann, A. Investigation of the shape-memory properties of 3D printed PLA structures with different infills. *Polymers* **2021**, *13*, 164. [[CrossRef](#)]
17. Ehrmann, G.; Ehrmann, A. Pressure orientation dependent recovery of 3D-printed PLA objects with varying infill degree. *Polymers* **2021**, *13*, 1275. [[CrossRef](#)]
18. Jia, S.K.; Yu, D.M.; Zhu, Y.; Wang, Z.; Chen, L.G.; Fu, L. Morphology, Crystallization and Thermal Behaviors of PLA-Based Composites: Wonderful Effects of Hybrid GO/PEG via Dynamic Impregnating. *Polymers* **2017**, *9*, 528. [[CrossRef](#)]
19. Wu, W.Z.; Ye, W.L.; Wu, Z.C.; Geng, P.; Wang, Y.L.; Zhao, J. Influence of layer thickness, raster angle, deformation temperature and recovery temperature on the shape-memory effect of 3D-printed polylactic acid samples. *Materials* **2017**, *10*, 970. [[CrossRef](#)]
20. Li, H.B.; Huneault, M.A. Effect of nucleation and plasticization on the crystallization of poly (lactic acid). *Polymer* **2007**, *48*, 6855–6866. [[CrossRef](#)]
21. Müller, A.J.; Ávila, M.; Saenz, G.; Salazar, J. Crystallization of PLA-based materials. In *Poly (Lactic acid) Science and Technology: Processing, Properties, Additives and Applications*; Jiménez, A., Peltzer, M., Ruseckaite, R., Eds.; RSC Polymer Chemistry Series No. 12; The Royal Society of Chemistry: Cambridge, UK, 2015.
22. Chalgham, A.; Wickenkamp, I.; Ehrmann, A. Mechanical properties of FDM printed PLA parts before and after thermal treatment. *Polymers* **2021**, *13*, 1239. [[CrossRef](#)]
23. Sölmann, S.; Rattenholl, A.; Blattner, H.; Ehrmann, G.; Gudermann, F.; Lütkemeyer, D.; Ehrmann, A. Mammalian cell adhesion on different 3D printed polymers with varying sterilization methods and acidic treatment. *AIMS Bioeng.* **2021**, *8*, 25–35.
24. Momeni, F.; Liu, X.; Ni, J. A review of 4D printing. *Mater. Des.* **2017**, *122*, 42–79. [[CrossRef](#)]
25. Kuang, X.; Roach, D.J.; Wu, J.T.; Hamel, C.M.; Ding, Z.; Wang, T.J.; Dunn, M.L.; Qi, H.J. Advances in 4d printing: Materials and applications. *Adv. Funct. Mater.* **2019**, *29*, 1805290. [[CrossRef](#)]
26. Sitotaw, D.B.; Ahrendt, D.; Kyosev, Y.; Kabish, A.K. Additive Manufacturing and Textiles—State-of-the-Art. *Appl. Sci.* **2020**, *10*, 5033. [[CrossRef](#)]
27. Koch, H.C.; Schmelzeisen, D.; Gries, T. 4D textiles made by additive manufacturing on pre-stressed textiles—An overview. *Actuators* **2021**, *10*, 31. [[CrossRef](#)]
28. Senatov, F.S.; Niaza, K.V.; Zadorozhnyy, M.Y.; Maksimkin, A.V.; Kaloshkin, S.D.; Estrin, Y.Z. Mechanical properties and shape memory effect of 3D printed PLA-based porous scaffolds. *J. Mech. Behav. Biomed. Mater.* **2016**, *57*, 139–148. [[CrossRef](#)]
29. Senatov, F.S.; Zadorozhnyy, M.Y.; Niaza, K.V.; Medvedev, V.V.; Kaloshkin, S.D.; Anisimova, N.Y.; Kiselevskiy, M.V.; Yang, K.-C. Shape memory effect in 3D printed scaffolds for self-fitting implants. *Europ. Polym. J.* **2017**, *93*, 222–231. [[CrossRef](#)]
30. Liu, W.B.; Wu, N.; Pochiraju, K. Shape recovery characteristics of SiC/C/PLA composite filaments and 3D printed parts. *Compos. Part A Appl. Sci. Manuf.* **2018**, *108*, 1–11. [[CrossRef](#)]

- 
31. Dong, J.; Mei, C.T.; Han, J.Q.; Lee, S.Y.; Wu, Q.L. 3D printed poly(lactic acid) composites with grafted cellulose nanofibers: Effect of nanofiber and post-fabrication annealing treatment on composite flexural properties. *Add. Manufact.* **2019**, *28*, 621–628. [[CrossRef](#)]
  32. Liu, Y.; Zhang, W.; Zhang, F.H.; Leng, J.S.; Pei, S.P.; Wang, L.Y.; Jia, X.Q.; Cotton, C.; Sun, B.Z.; Chou, T.-W. Microstructural design for enhanced shape memory behavior of 4D printed composites based on carbon nanotube/poly(lactic acid) filament. *Compos. Sci. Technol.* **2019**, *181*, 107692. [[CrossRef](#)]